Photochemical & Photobiological Sciences

Accepted Manuscript

This is an *Accepted Manuscript*, which has been through the Royal Society of Chemistry peer review process and has been accepted for publication.

Accepted Manuscripts are published online shortly after acceptance, before technical editing, formatting and proof reading. Using this free service, authors can make their results available to the community, in citable form, before we publish the edited article. We will replace this *Accepted Manuscript* with the edited and formatted *Advance Article* as soon as it is available.

You can find more information about *Accepted Manuscripts* in the Information for Authors.

Please note that technical editing may introduce minor changes to the text and/or graphics, which may alter content. The journal's standard Terms & Conditions and the Ethical guidelines still apply. In no event shall the Royal Society of Chemistry be held responsible for any errors or omissions in this *Accepted Manuscript* or any consequences arising from the use of any information it contains.

ROYAL SOCIETY OF CHEMISTRY

www.rsc.org/pps

Journal Name

RSCPublishing

ARTICLE

The effect of diketopyrrolopyrrole (DPP) group inclusion in *p*-cyanophenyl end-capped oligothiophene used as dopant in P3HT:PCBM BHJ solar cells

Cite this: DOI: 10.1039/x0xx00000x

Received 00th April 2014,
Accepted 00th April 2014

DOI: 10.1039/x0xx00000x

www.rsc.org/

V. M. Manninen,[a] J. P. Heiskanen,[b] D. Pankov,[b] T. Kastinen,[a] T. I. Hukka,[a] O. E. O. Hormi [b] and H. J. Lemmetyinen[a]

In this work, two *p*-cyanophenyl end-capped oligothiophenes, **DPP-(2TPhCN)$_2$** and **di-(*p*-CNPh)4T**, were compared as dopants in the P3HT:$PC_{60}BM$ bulk heterojunction (BHJ) layer of inverted organic solar cells. Inclusion of **DPP-(2TPhCN)$_2$** significantly increased the average efficiency of the solar cells, while the increase using **di-(*p*-CNPh)4T** doping on the cell efficiency was minor. In the BHJ photoactive layer, the dopant molecules are close to and interact with P3HT and $PC_{60}BM$ molecules. Intra- and intermolecular interactions of the dopant molecules with P3HT and $PC_{60}BM$ were studied in chloroform solutions. Energy or electron transfer from the dopant molecules to $PC_{60}BM$ takes place, as the fluorescence emission intensity and lifetime of the dopant molecules decreased in the presence of $PC_{60}BM$. In the case of doping with **DPP-(2TPhCN)$_2$**, doped cells had higher absorbance than the non-doped reference cell and doping broadens the cell absorption to the near IR-region. Thus, the dopant molecules act as additional light absorbers in the photoactive layer and transfer energy or electrons to $PC_{60}BM$, which increases the short circuit current and power conversion efficiency of the cell. Also, the emission of the cells doped with **DPP-(2TPhCN)$_2$** decreased when compared to that of the reference cell. In this case, P3HT can give electrons or energy to dopant molecules and the cell current and efficiency are further increased.

Introduction

Recently, diketopyrrolopyrrole (DPP)-based materials have been widely studied in both polymer[1] and small molecule[2] bulk heterojunction (BHJ) organic solar cells (OSCs). The DPP-core is one of the most attractive units for tailored photovoltaic materials since the molecular properties can be greatly affected by attaching different side groups to the DPP-core. The conjugated planar DPP-core provides high hole mobility for donor materials. By attaching electron donating side groups, *e.g.* thiophenes, low band-gap high performance donor materials have been synthesized for BHJ OSCs.[2] DPP-based acceptor materials for BHJ OSCs have been synthesized by attaching side groups with electron withdrawing end-capping groups, *e.g.* trifluoromethylphenyl, to the DPP core.[3] DPP-containing oligothiophene-fullerene triads have been synthesized and used as photoactive layer material on their own or together with poly(3-hexylthiophene) (P3HT) in BHJ OSCs.[4] Apart from their use in OSCs, metal-free dyes with DPP-cores have been synthesized for use in efficient dye-sensitized solar cells.[5]

In addition to their excellent photovoltaic performance, DPP-based materials have interesting photophysical properties. When electron-donating oligothiophene side groups are attached to the electron-deficient DPP-core, the band gap is reduced, which extends the light absorption into the near-infrared region. A common feature of DPP-based materials is their relatively high oxidation potential, which leads to a high-energy charge separated state, when combined with fullerenes. Correspondingly, high voltages are produced when the materials are used in OSCs. One of the drawbacks of the low band gap DPP-based molecules is their generally low triplet state energy.[6,7] If the triplet energy is lower than the energy of the charge separated state, the charge recombination to the triplet state is possible. The triplet recombination is a likely loss mechanism in OSCs based on low band gap donor materials.[8]

Because the DPP-based materials absorb at longer wavelengths than P3HT, their inclusion as additional dopant molecules in the P3HT:$PC_{60}BM$ photoactive layer broadens the absorption band of the BHJ solar cells. As DPP-based materials can function as donor materials, it is likely that they interact with $PC_{60}BM$. Inclusion of different dopant molecules in the photoactive layer of P3HT:$PC_{60}BM$ BHJ OSCs has been widely studied. The improved efficiency of cells using various low band gap materials, such as DPP- or naphthalene based small molecules,[9] or metal complexes, such as Alq_3 derivatives,[10] has been reported. Improvements in the efficiency of the doped cells have been attributed to advantageous active layer morphology changes, increased P3HT crystallization, wider absorption area and improved charge transport in the photoactive layer. Interaction of dopant molecules, such as fluorescence resonance energy transfer (FRET), with active layer components was reported[11] to significantly improve the cell efficiency. However, further fundamental research and

better understanding of the functional principles of the doped cells is required. This can be done by utilizing detailed spectroscopic studies of dopant/$PC_{60}BM$ and dopant/P3HT interactions.

Previously, we studied the interaction of an Alq_3 end-capped oligothiophene, $(Alq_3)_2$-OT, with $PC_{60}BM$ using steady state and time resolved spectroscopic methods.[12] As the electron transfer from the $(Alq_3)_2$-OT to $PC_{60}BM$ was observed, $(Alq_3)_2$-OT was applied as a dopant material in the P3HT:$PC_{60}BM$ photoactive layer of inverted BHJ organic solar cells. $(Alq_3)_2$-OT dopant molecules served as additional donor molecules in the photoactive layer and increased the cell current and efficiency by donating electrons to $PC_{60}BM$.

In this work, we studied the interactions of two aryl end-capped small molecule donor materials, **DPP-(2TPhCN)$_2$** and **di-(*p*-PhCN)T4** (Fig. 1), with the photoactive layer components, P3HT and $PC_{60}BM$. **DPP-(2TPhCN)$_2$** was synthesized in order to include a DPP-group in the aryl end-capped oligothiophene. These two compounds were compared as dopant materials in inverted P3HT:$PC_{60}BM$ BHJ OSCs. The **DPP-(2TPhCN)$_2$** doping improved the cell efficiency, while the influence of the **di-(*p*-PhCN)T4** doping on the cell efficiency was minor. The effect of the dopant materials on the cell efficiency is explicable based on the performed spectroscopic measurements.

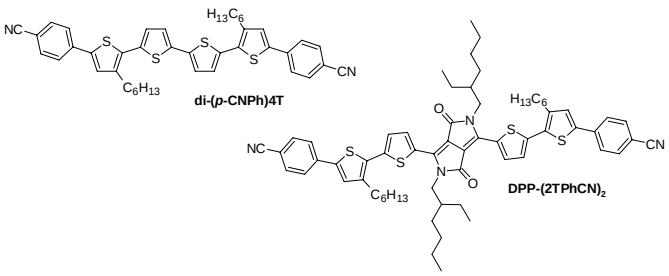

Fig. 1 Chemical structures of **di-(p-CNPh)4T** and **DPP-(2TPhCN)$_2$**.

Results and discussion

Synthesis of DPP-(2TPhCN)$_2$

A recently reported direct arylation method of a DPP unit with various aryl halides and thiophene derivatives[13] was inefficient in our hands. Following the direct coupling protocol, coupling of the commercial starting material **1** with 2-hexylthiophene gave the compound **2** only in 34% yield. After a short optimization series (Table 1), compound **2** could be prepared by a Suzuki-Miyaura cross-coupling between compound **1** and 3-hexylthiophene-2-boronic acid pinacol ester. The standard $Pd(PPh_3)_4$ catalyst together with toluene/DMA/H_2O solvent mixture gave the best result (entry 3). Compound **2** was isolated in high yield by column chromatography.

Compound **2** was brominated using *N*-bromosuccinimide (NBS) (2.1 equiv) under ultrasound irradiation. The compound **3** was produced in 75% yield when the reaction was carried out in toluene. However, the yield could be improved to 97% by using chloroform as a reaction solvent.

Table 1 Optimization of Suzuki-Miyaura cross-coupling of compound **1** with 3-hexylthiophene-2-boronic acid pinacol ester.

Entry	Catalyst	Ligand	Solvent	Time	Yield[a]
1	$Pd(dppf)Cl_2$	-	toluene/ DMA/H_2O	1	74.5
2	$Pd_2(dba)_3$[b]	*t*-$Bu_3P{\cdot}HBF_4$[c]	toluene/ DMA/H_2O	2	86.2[d]
3	$Pd(PPh_3)_4$	-	toluene/ DMA/H_2O	2	92.4[d,e]
4	$Pd(PPh_3)_4$	-	DMA/H_2O	3 ½	26

Reaction conditions: catalyst 12 mol%, Cs_2CO_3 (4.5 equiv), 3-hexylthiophene-2-boronic acid pinacol ester (2.1 equiv), 110 °C, [a]Isolated yield of compound **2**, [b]6 mol%, [c]24 mol%, [d]Average of three runs, [e]The highest yield was 94%.

The optimized reaction conditions for the first reaction step were also usable for the Suzuki-Miyaura cross-coupling between compound **3** and 4-cyanophenylboronic acid. However, the standard $Pd(PPh_3)_4$ catalyst only gave the **DPP-(2TPhCN)$_2$** in moderate yield (44%) while using Pd_2dba_3 as a palladium source with *t*-$Bu_3P{\cdot}HBF_4$ as a ligand gave the target compound **DPP-(2TPhCN)$_2$** in a good yield (84%).

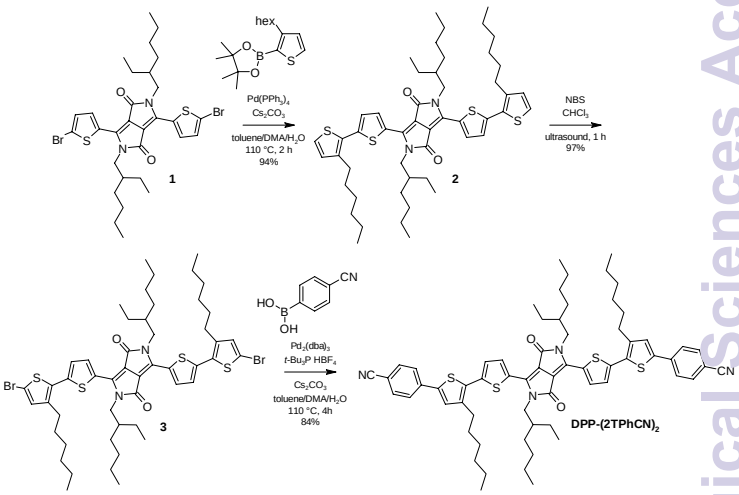

Scheme 1 Synthesis of **DPP-(2TPhCN)$_2$**.

Computational modeling of DPP-(2TPhCN)$_2$

The DFT-optimized ground-state geometry of **DPP-(2TPhCN)$_2$** is shown in Fig. 2. The dihedral angles (the C-C-C-C dihedral angles, α in Fig. 2) between the thiophenes and the terminal phenyl groups are 20° and 23°. The long hexyl side chains twist the backbone as well, resulting in the dihedral angles of 167° and 153° between adjacent thiophenes (the C-C-C-C dihedral angles, β in Fig. 2), i.e. the neighboring sulfur atoms are *anti* to each other. However, the dihedral angles between the thiophenes and the DPP-core (the C-C-C-C dihedral angles, γ in Fig. 2) are only 9° and 1°. This can be attributed to the planarizing effect of the hydrogen bonds between the carbonyl groups of the DPP-core and the hydrogen atoms of the neighboring thiophenes.[14,15] The bulky 2-ethylhexyl side chains of the DPP-core have been shown to induce an additional twist to the backbone,[16] but their effect is here not as significant as in ref. 13. This is most probably due to the different geometries and side-chain positioning of the compounds. Additionally, the differences between the measuring methods (i.e. gas-phase DFT calculation versus condense phase single crystal X-ray diffraction measurement) may have some effect.[14] More accurate values of the dihedral angles are presented in Figure S1 and Table S1.

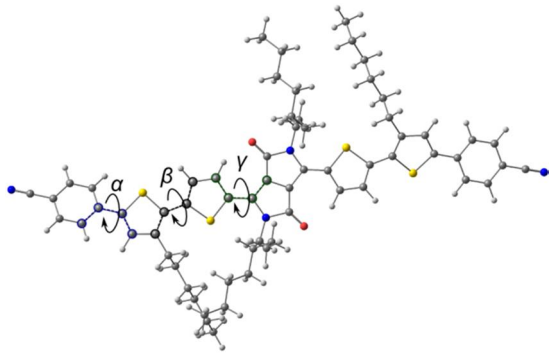

Fig. 2 Optimized ground-state geometry of **DPP-(2TPhCN)$_2$** calculated at the B3LYP/6-31G** level of theory.

The calculated energies of the HOMO and LUMO levels and the HOMO-LUMO gap energies of **DPP-(2TPhCN)$_2$** are presented in Table 2. The calculated HOMO and LUMO levels are slightly higher than the experimental values measured by differential pulse voltammetry (DPV). The computed frontier molecular orbitals are shown in Fig. 3. Both the HOMO and LUMO are mainly localized on the backbone with only a small amount of electron density on the terminal phenyl groups. In the HOMO, ca. 96% of the molecular orbital is localized on the backbone and only 4% on the terminal phenyl groups (Table S2). Part of the electron density is transferred from the backbone to the terminal groups upon excitation. Consequently, ca. 91% of the LUMO is on the backbone and 9% on the terminal phenyl groups.

Table 2 HOMO, LUMO and band gap (E_g) energies of **DPP-(2TPhCN)$_2$** calculated at the B3LYP/6-31G** level of theory and obtained by DPV measurements.

Method	HOMO (eV)	LUMO (eV)	E_g (eV)
DFT	-5.0	-2.9	2.0
DPV	-5.2	-3.3	1.9

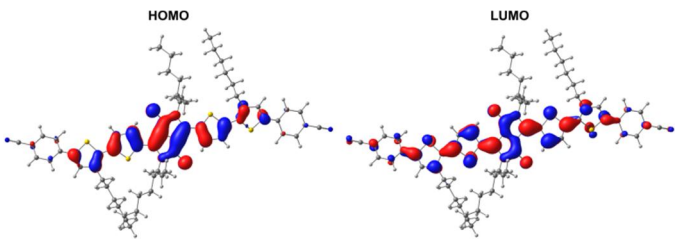

Fig. 3 Frontier molecular orbitals of **DPP-(2TPhCN)$_2$** calculated at the B3LYP/6-31G** level of theory (isodensity contour = 0.025).

The more precise contributions of the DPP and thiophene units into the HOMO are 54% and 43%, respectively, and into the LUMO 38% and 53%, respectively. Thus, it could be assumed that electron density is transferred from the DPP-core to the thiophenes and the terminal phenyl groups upon excitation. Intramolecular charge transfer was computed in detail (See SI: Fig. S3 and Table S3) and its properties are discussed in the next section. However, caution must be used in drawing conclusions based on these results, because there is no universally agreed best method to determine the contributions of molecular fragments to the molecular orbitals and different population analysis methods result in different values.[17,18]

Computational calculations have been performed on **di-(*p*-PhCN)T4** before[19] (Frontier molecular orbitals, See: Fig. S4; Contributions to the HOMO and LUMO, See Table S4). The HOMO electron density of **di-(*p*-PhCN)T4** concentrated on the quaterthiophene backbone. Upon excitation, the electrons moved from the electron donating quaterthiophene backbone to the electron deficient end-capped *p*-cyanophenyl groups.

Absorption properties of DPP-(2TPhCN)$_2$

The properties of different thiophene groups attached to the DPP-core have been studied extensively[6,Error! Bookmark not defined.,7] and have a significant effect on the number and positions of the molecule absorption bands. In the literature, two characteristic longer wavelength maxima of the DPP-core with bithiophene side groups peaked at around 580 and at 617 nm and the shorter wavelength maxima were at 350 nm and 410 nm.[6] The band at 410 nm was characterized as an intramolecular charge transfer (ICT) band as electrons move from the terminal donor groups to the DPP-core. A gradual red shift of the ICT band increased with the electron rich nature of the aromatic groups end-capped to the bithiophene side groups of the DPP-core. When trithiophene groups were attached to the DPP-core, the short wavelength absorptions peaked at 325 nm and 390 nm, a shoulder appeared at around 450 nm and the long wavelength absorptions were at 610 nm and 661nm.[20]

As **DPP-(2TPhCN)$_2$** is end-capped with electron withdrawing[20] *p*-cyanophenyl groups, the long wavelength absorption of **DPP-(2TPhCN)$_2$** (Fig. 4a) is red-shifted compared to that of the DPP-core with bithiophene side groups.[6] The spectrum of **DPP-(2TPhCN)$_2$** peaks at 600 nm and has a vague shoulder at 650 nm, which results in a 1.9 eV optical band gap energy calculated from the shoulder. The value of the optical band gap is the same as the electrochemical band gap measured by DPV, but the computational calculations gave a slightly larger gap of 2.0 eV. The short wavelength absorption band of **DPP-(2TPhCN)$_2$** at 325 nm corresponds to the reported[7] absorption of a DPP-core with trithiophene side groups. This indicates that the conjugation in the thiophene parts of **DPP-(2TPhCN)$_2$** is extended partly to cover the aryl groups, which provides side group absorption that corresponds that of trithiophene side groups.

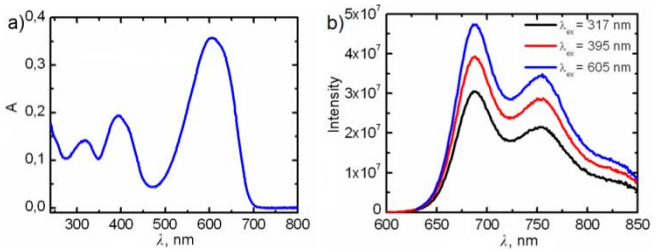

Fig. 4 Absorption (a) and fluorescence emission (b) spectra of 1.13 μM **DPP-(2TPhCN)$_2$** in chloroform.

The computational calculations support a charge transfer from the DPP-core and thiophenes to the terminal *p*-cyanophenyl groups in the excited state of **DPP-(2TPhCN)$_2$**. According to the DFT calculations (Table S3 and Figure S3), the **DPP-(2TPhCN)$_2$** absorption band at 428 nm (Fig. S2) corresponds to two electronic configurations. The one (~53%), in which the electron density is transferred from the whole oligomer towards the DPP-core, and another (~45%), in which the electron density moves from the DPP-core and the thiophenes to the end-capped aryl groups. The **DPP-(2TPhCN)$_2$** absorption band at 400 nm corresponds to the calculated band at 428 nm, as the used computational method red-shifts the bands. Thus, the band

at 400 nm is assigned as an ICT band, which was observed in the transient absorption measurements (Fig. 14), and is discussed in detail in the last section. Fluorescence emission spectra of **DPP-(2TPhCN)$_2$** excited at each absorption maximum (317 nm, 395 nm and 605 nm) show the emission maxima at 690 nm and 750 nm (Fig. 4b), which corresponds the reported[7] emission of the DPP-core with trithiophene side groups.

Electrochemical properties of DPP-(2TPhCN)$_2$

DPV curves of **DPP-(2TPhCN)$_2$** and ferrocene are shown in Fig. 5. Two reversible oxidations, at 0.65 V and 0.81 V, and three reversible reductions, at -1.22 V, -1.63 V and -1.97 V, were observed. The HOMO and LUMO energy levels of **DPP-(2TPhCN)$_2$**, based on the first oxidation and reduction potentials referenced to the ferrocene oxidation potential are -5.2 eV and -3.3 eV, respectively. Electrochemical band gap is 1.9 eV.

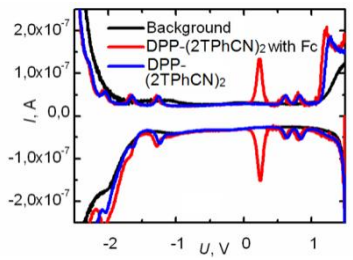

Fig. 5 DPV curves of **DPP-(2TPhCN)$_2$** and ferrocene reference in dichloromethane.

Solar cell experiments

DPP-(2TPhCN)$_2$ and **di-(*p*-CNPh)4T** were compared as dopants in the photoactive layer of the inverted ITO|ZnO|P3HT:$PC_{60}BM$|Alq_3|Ag (Fig. 6) OSC. Different mass ratios of the dopants and other components, P3HT donor and $PC_{60}BM$ acceptor, were tested in the photoactive BHJ layer.

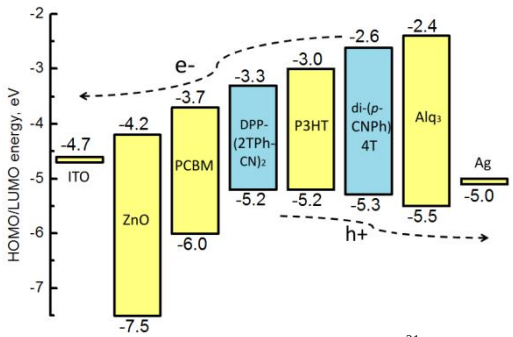

Fig. 6 Energy levels of the inverted cell structure[21] (yellow) and the used dopant molecules **DPP-(2TPhCN)$_2$** and **di-(*p*-CNPh)4T** (blue). Direction of the electron and hole transport is shown by arrows.

Photovoltaic parameters of the reference cell, the cells with 2.5–10 m% of **DPP-(2TPhCN)$_2$** dopant in the P3HT:$PC_{60}BM$ photoactive layer and a **DPP-(2TPhCN)$_2$**:PC_{70} BM cell (60:40) cell are shown in Table 3 and the *I-V* curves in Fig. 7. The use of **DPP-(2TPhCN)$_2$** as a dopant molecule improved the cell power conversion efficiency (η), when the mass of dopant molecules in the photoactive layer was 3.5% or 5.0% of the P3HT:$PC_{60}BM$:dopant mixture total mass. Efficiencies of the best cells doped with 3.5 m% or 5.0 m% of **DPP-(2TPhCN)$_2$** in the photoactive layer were 3.0% and 3.3%, respectively, compared to 2.8% efficiency of the best reference cell measured one day after cell preparation. The average efficiency of the cells, when the amount of the dopant molecules was 3.5 m%, was 2.7% compared to 2.4% average efficiency of non-doped reference cells.

Table 3 The amount of **DPP-(2TPhCN)$_2$** dopant molecules (2.5–10 m%) in the photoactive layer of the P3HT:$PC_{60}BM$ cell, the corresponding photovoltaic parameters measured one day after cell preparation and their standard deviations, and those of the **DPP-(2TPhCN)$_2$**:$PC_{70}BM$ (60:40) cell.

m%	mol%	n[a]	$I_{sc,\,best}$ (mA/cm^2)	$V_{oc,best}$ (V)	FF_{best} (%)	η_{best} (%)	η_{avg} (%)
0	**0**	9	-2.9±0.14	0.55±0.008	57±6.3	2.8±0.35	2.4±0.35
2.5	**0.7**	9	-2.5±0.25	0.54±0.008	62±7.2	2.5±0.29	2.1±0.29
3.5	**1.0**	10	-2.9±0.16	0.55±0.004	58±8.2	3.0±0.24	2.7±0.24
5.0	**1.4**	10	-3.3±0.29	0.54±0.010	62±6.7	3.3±0.41	2.6±0.41
6.5	**1.8**	9	-2.7±0.31	0.55±0.003	53±6.6	2.5±0.43	2.0±0.43
10	**2.7**	7	-1.9±0.24	0.55±0.008	41±4.1	1.3±0.08	1.2±0.08
60[b]	**59**	4	-1.2±0.23	0.61±0.036	34±2.1	0.7±0.10	0.6±0.10

[a]Number of solar cell samples, [b]**DPP-(2TPhCN)$_2$**:$PC_{70}BM$ (60:40) cell

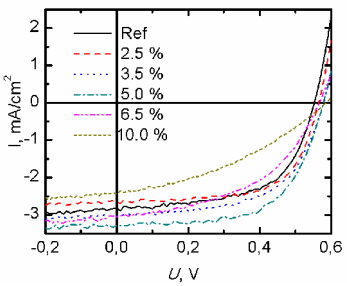

Fig. 7 *I-V* curves of the P3HT:$PC_{60}BM$ reference cell and the cells doped with **DPP-(2TPhCN)$_2$** (in m%, as in Table 3) measured one day after cell preparation.

The cells were re-measured one month after cell preparation and the photovoltaic parameters are shown in Table 4. During the storage in dark, the efficiencies of the best cells with 3.5 m% and 5.0 m% of **DPP-(2TPhCN)$_2$** dopant increased to 3.2% and 3.6%, respectively, compared to the 2.8% efficiency of the reference cell. The average efficiency of the cells with 5.0 m% of **DPP-(2TPhCN)$_2$** dopant increased to 2.9% compared to 2.4% average of the reference cells. These results demonstrate the long-term stability of the prepared inverted cells.

Inclusion of **DPP-(2TPhCN)$_2$** dopant molecules in the photoactive layer does not change the cell V_{oc} remarkably. The cell efficiency is primarily improved due better I_{sc} and slightly higher *FF* values. When the content of the dopant molecules is 6.5 m% or more, the morphology of the P3HT:$PC_{60}BM$ layer seems to deteriorate, since aggregates could be seen in the BHJ layer by an optical microscope. Large concentrations of the dopant molecules possibly prevent the formation of the continuous paths of hole transporting P3HT and electron transporting $PC_{60}BM$ phases. Thus, the efficiency of the cell probably decreases due to decreased charge transport to the electrodes.

The **DPP-(2TPhCN)$_2$**:$PC_{70}BM$ (60:40) cell, where P3HT was completely replaced by **DPP-(2TPhCN)$_2$** as a donor material in the BHJ layer, had an efficiency of 0.7% after optimization experiments. The theoretical maximum efficiency for the cell, with the same donor LUMO and PCBM acceptor

and *FF* being 65%, is ~4-5%.[22] The cell had a V_{oc} of 0.61 V, which corresponds well with the V_{oc} produced by the donors with the same HOMO level.[22] I_{sc} and *FF* remained low, which limited the cell function. Perhaps **DPP-(2TPhCN)$_2$** is able to donate electrons to $PC_{60}BM$ to certain extent. But, whether the charge separation is inefficient, recombination back to **DPP-(2TPhCN)$_2$** triplet state is fast, or a decent BHJ network with $PC_{70}BM$ is not formed. Any of these could possibly decrease the charge transport to the electrodes.

Table 4 The content (2.5–10 m%) of **DPP-(2TPhCN)$_2$** dopant molecules in the photoactive layer of the P3HT:$PC_{60}BM$ cell, the corresponding photovoltaic parameters measured one month after cell preparation and their standard deviations.

m%	mol%	n*	$I_{sc,\,best}$ (mA/cm^2)	$V_{oc,best}$ (V)	FF_{best} (%)	η_{best} (%)	η_{avg} (%)
0	**0**	9	-2.8±0.17	0.54±0.012	61±4.7	2.8±0.27	2.4±0.27
2.5	**0.7**	8	-2.7±0.30	0.56±0.007	65±9.4	3.0±0.55	2.3±0.55
3.5	**1.0**	9	-3.0±0.19	0.57±0.003	59±3.4	3.2±0.21	2.8±0.21
5.0	**1.4**	9	-3.3±0.36	0.57±0.005	62±7.0	3.6±0.59	2.9±0.59
6.5	**1.8**	9	-3.1±0.44	0.56±0.007	49±10	2.6±0.64	1.9±0.64
10	**2.7**	4	-2.4±0.55	0.58±0.032	38±3.7	1.7±0.35	1.2±0.35

*Number of the measured samples

Doping the P3HT:$PC_{60}BM$ cell with **DPP-(2TPhCN)$_2$** broadens the cell absorbance (Fig. 8a) to the longer wavelengths, which is one possible explanation for the increased cell I_{sc}. In addition, the emission of P3HT in the doped cells is decreased when compared to the reference cell (Fig. 8b). Most probably, P3HT can give electrons or to dopant molecules and the cell current and efficiency are further increased (See SI: p. 20).

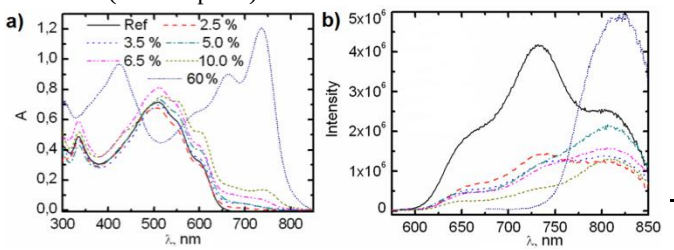

Fig. 8 Absorption (a) and emission (b) (λ_{ex} = 500 nm) spectra of the P3HT:$PC_{60}BM$ reference cell and the cells doped with **DPP-(2TPhCN)$_2$** (in m%, as in Table 3) and those of the **DPP-(2TPhCN)$_2$**:$PC_{70}BM$ (60:40) cell, (λ_{ex} = 660nm). The legends in (a) correspond to those in (b).

The cell photocurrent spectra in Fig. 9 clearly show, that the cell with 5 % content of **DPP-(2TPhCN)$_2$** produces more current than the undoped reference cell at the wavelength range from 625 nm to 800 nm. However, the photocurrent produced by the doped cell and the reference cell are nearly the same at the wavelength range from 450 nm to 625 nm. This clearly shows, that the absorption of the dopant molecules leads to additional current production in the doped cells at longer wavelengths.

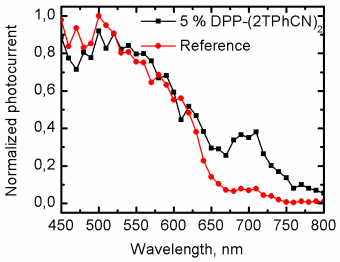

Fig. 9 Normalized photocurrent spectra of the solar cell sample with 5 % content of DPP-(2TPhCN)$_2$ (black squares) and the reference cell (red circles).

For comparison, **di-(*p*-CNPh)4T** was used as a dopant molecule in the photoactive layer in three similar molar ratios (0.7, 1.4 and 2.7) to **DPP-(2TPhCN)$_2$**. Only one cell out of ten **di-(*p*-CNPh)4T** doped cells showed improved efficiency compared to the reference cell when the content of dopant molecules was 4.8 m% (Table 5, Fig. 10). The average efficiency of the cells was not improved using any of the tested **di-(*p*-CNPh)4T** dopant concentrations compared with the average efficiency of the undoped reference cells measured one day after cell preparation.

After one month of storage, the average efficiencies of the cells with 2.4 m% or 3.6 m% content of **di-(*p*-CNPh)4T** dopant were slightly improved compared to the average efficiency of the reference cells (Table 6). When **di-(*p*-CNPh)4T** was used as a donor material, completely replacing P3HT, the best efficiency after optimization experiments was 0.1%. The theoretical maximum efficiency for the cell, with the same donor LUMO level and PCBM acceptor, is less than 1%.[22] A high V_{oc} of 0.67 V was produced, but the I_{sc} was only -0.12 mA/cm^2. Possibly, the poor performance of the **di-(*p*-CNPh)4T**:$PC_{60}BM$ cell is due to inefficient electron transfer between the molecules, poor charge mobility in the **di-(*p*-CNPh)4T** phase or poor phase separation in the BHJ layer.

Table 5 The content (2.4–4.8 m%) of **di-(*p*-CNPh)4T** dopant molecules in the photoactive layer of the P3HT:$PC_{60}BM$ reference cell, the corresponding photovoltaic parameters measured one day after the cell preparation and their standard deviations, and those of the **di-(*p*-CNPh)4T:**$PC_{60}BM$ (67:33) cell.

m%	mol%	n[a]	$I_{sc,best}$ (mA/cm^2)	$V_{oc,best}$ (V)	FF_{best} (%)	η_{best} (%)	η_{avg} (%)
0	**0**	7	-2.9±0.27	0.55±0.011	56±7.1	2.8±0.44	2.6±0.44
2.4	**0.7**	5	2.6±0.26	0.54±0.004	57±7.9	2.5±0.04	2.5±0.04
3.6	**1.4**	6	-3.5±0.42	0.54±0.005	46±9.5	2.7±0.53	2.5±0.53
4.8	**2.7**	10	-3.4±0.29	0.53±0.006	62±5.6	3.5±0.46	2.5±0.46
67[b]	**73**	3	-0.1±0.05	0.67±0.000	42±16	0.1±0.04	0.1±0.04

[a]Number of solar cell samples, [b]**di-(*p*-CNPh)4T**:$PC_{60}BM$ (67:33) cell

Table 6 The content (2.4–4.8 m-%) of **di-(*p*-CNPh)4T** dopant molecules in the photoactive layer of the P3HT:$PC_{60}BM$ reference cell, the corresponding photovoltaic parameters measured one month after cell preparation and their standard deviations.

m%	mol%	n*	$I_{sc,best}$ (mA/cm^2)	$V_{oc,best}$ (V)	FF_{best} (%)	η_{best} (%)	η_{avg} (%)
0	**0**	7	-3.0±0.25	0.55±0.005	60±4.9	3.0±0.37	2.6±0.37
2.4	**0.7**	8	-2.9±0.23	0.54±0.012	57±3.4	2.8±0.14	2.6±0.14
3.6	**1.4**	5	-3.1±0.40	0.56±0.009	57±2.8	3.0±0.42	2.6±0.42
4.8	**2.7**	9	-3.4±0.28	0.54±0.004	62±5.4	3.5±0.43	2.6±0.43

*Number of the measured samples

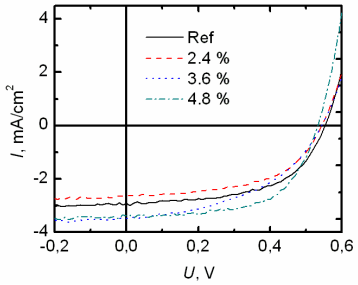

Fig. 10 *I-V* curves of the P3HT:$PC_{60}BM$ cells doped with **di-(*p*-CNPh)4T** (in m%, as in Table 5).

The cell absorption spectra show increased absorption due to the **di-(*p*-CNPh)4T** doping, when 3.6 m% of the dopant is used (Fig. 11a). However, absorbances of the cells with 2.4 m% or 4.8 m% of the dopant decrease compared to the reference cells. These differences might be due to uneven spin-coated films. The emission of P3HT is not quenched in the cells doped with **di-(*p*-CNPh)4T** (Fig. 11b) as it was in the case of **DPP-(2TPhCN)$_2$** doping. In contrast, the cell emission intensities increase in the presence **di-(*p*-CNPh)4T**. This could be due to increased P3HT recombination as a result of poor film quality. Since the emission of the dopant molecules is not visible in the cell emission spectra, the dopant molecules probably give electrons to P3HT (See SI: pp. 21-22), but this does not contribute to increased current production, because P3HT is a hole conductor.

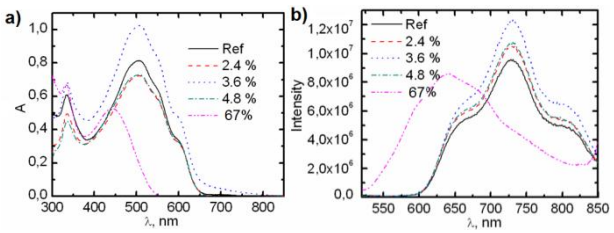

Fig. 11 Absorption (a) and emission (b) spectra (λ_{ex} =500 nm) of the P3HT:$PC_{60}BM$ reference cell and the cells doped with **di-(*p*-CNPh)4T** (in m%, as in Table 5) as well as those of the **di-(*p*-CNPh)4T**:$PC_{60}BM$ (67:33) cell (λ_{ex} = 450 nm).

Absorption and fluorescence properties of DPP-(2TPhCN)$_2$ in the presence of $PC_{60}BM$ and P3HT.

Doping of organic solar cells means the insertion of additional dopant molecules into the solution of photoactive layer components, P3HT and $PC_{60}BM$, and spin coating of the solution. After the spin coating the dopant molecules form with P3HT and $PC_{60}BM$ a solid BHJ layer, where the molecules are mixed and in close proximity. This interaction can be easily observed from the broadened and red shifted absorption and emission spectra of the cells (Fig. 8 and 11) compared to those measured in solution (Figures 12a and 15a). Thus, intermolecular interactions, such as energy or electron transfer, are possible between the molecules in solid cell structures. Interactions of **DPP-(2TPhCN)$_2$** and **di-(*p*-CNPh)T4** dopant molecules with P3HT and $PC_{60}BM$ were studied by steady state and time-resolved absorption and fluorescence methods in chloroform solutions.

Interaction of DPP-(2TPhCN)$_2$ with $PC_{60}BM$. When 0.12 mM **DPP-(2TPhCN)$_2$** is mixed with different concentrations of $PC_{60}BM$ in chloroform, their combined emission intensity decreases as a function of the $PC_{60}BM$ concentration as shown in Table 7 and Fig. 12. Also, lifetimes in the single exponential fits of the fluorescence decay curves (Fig. 13a, Table 7) decrease as the $PC_{60}BM$ concentration increases. The decrease in the fluorescence intensities, which are corrected due to the increased absorbance, is larger relative to the decrease in the measured lifetimes. This is partly due to a decrease in the absorption of **DPP-(2TPhCN)$_2$** as a consequence of the high absorbance of $PC_{60}BM$ at the excitation wavelength, 650 nm (Fig. 12a). The emission of **DPP-(2TPhCN)$_2$** is possibly dynamically quenched by $PC_{60}BM$.[23] The rate constant for the dynamic quenching can be determined based on changes in the fluorescence lifetimes as a function of the $PC_{60}BM$ concentration. As (Fig. 13b) $\tau_0/\tau = 1 + K_D[Q]$, K_D = 0.026 M-1/10^{-3} = 26 M^{-1}, the dynamic quenching rate constant, k_q = 26 M^{-1}/1.08 ns = 2.40×10^{10} M^{-1} s^{-1}. This value corresponds well the diffusion controlled rate constant in chloroform. Thus the quenching of **DPP-(2TPhCN)$_2$** with $PC_{60}BM$ is possible, either via the energy or electron transfer mechanism.

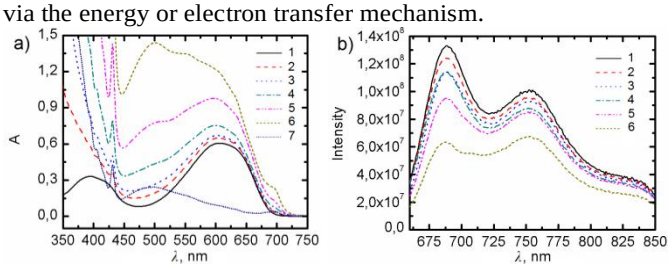

Fig. 12 Absorption (a) and emission (λ_{ex} = 650 nm) (b) spectra of **DPP-(2TPhCN)$_2$** with different concentrations of $PC_{60}BM$ in $CHCl_3$ solutions 1–7. Concentrations of **DPP-(2TPhCN)$_2$** and $PC_{60}BM$ in solutions 1–7 are shown in Table 7.

Table 7. Concentrations, absorbances at the excitation wavelength, transmittances at the excitation wavelength, measured and corrected fluorescence emission (λ_{ex} = 650 nm) intensities at 750 nm, and fluorescence lifetimes (λ_{mon} = 690 nm) of **DPP-(2TPhCN)$_2$** (DPP) and $PC_{60}BM$ (Q) solutions 1–7 (Fig. 12) in chloroform.

Solution/ Curves	[DPP] (mM)	[Q] (mM)	$A_{(650)}$	$T_{(650)}$[a]	$I_{(750)}$ (10^7)	$I_{corr(750)}$ (10^8)	$\tau_{(690)}$ (ns)
1	0.12	-	0.44	0.60	10	2.5	1.08
2	0.12	0.44	0.47	0.58	9.5	2.3	1.07
3	0.12	0.88	0.48	0.57	8.8	2.1	1.06
4	0.12	1.76	0.52	0.55	9.2	2.1	1.03
5	0.12	3.52	0.67	0.46	8.4	1.6	1.00
6	0.12	7.04	0.70	0.45	6.7	1.2	0.91
7	-	0.15	0.01	-	-	-	-

[a]Estimated transmittance of the sample solution for the excitation light: $T_{ex} = 10^{(-1/2\times A(650))}$, as the fluorescence intensity is measured in 90 degree angle relative to excitation, [b]Corrected intensity at 750 nm: $I_{corr} = I_{(750)}/(1-T_{ex})$

In the fluorescence lifetime experiments above, the excitation took place at 650 nm, where mainly the DPP-core absorbs. The lifetime of the DPP-group alone is 7.1 ns[24], but it is reduced in the case of **DPP-(2TPhCN)$_2$**, due to the attached substituted thiophene side groups, to 1.1 ns. Thus, intramolecular quenching takes place and corresponds to the charge transfer from the DPP-core to the attached aryl end-capped thiophene side groups.

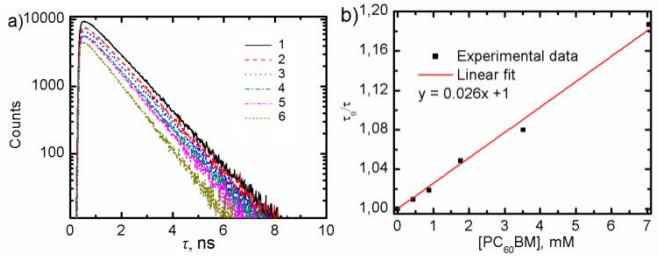

Fig. 13 Fluorescence decay curves (λ_{ex} = 650 nm and λ_{mon} = 690 nm) (a) and τ_0/τ as a function of $PC_{60}BM$ concentration (b) of the **DPP-(2TPhCN)$_2$** and $PC_{60}BM$ solutions.

In order to study the intramolecular electron transfer of the **DPP-(2TPhCN)$_2$** molecule, which should take place according to the molecular modeling discussed above, pump-probe experiments were performed in chloroform. The excitation took place at 650 nm, where only the DPP-moiety absorbs. Fig. 14a presents the sum of the decay component spectra of **DPP-(2TPhCN)$_2$** in chloroform at 0 ps (green curve) and the component spectra with lifetimes of 6.2 ps and 590 ps (blue and red curves) in the visible light region, and 9.8 ps and 740 ps in the near-infrared region. It is worth noticing, that none of the lifetimes observed here correspond to the fluorescence lifetime (≈ 1.1 ns) measured by the single photon counting method discussed above. A transient state is formed in 8.0 ps, average of the both wavelength ranges, which can be seen as a bleaching of the **DPP-(2TPhCN)$_2$** ground state (blue triangles) at 550–650 nm and a low positive band at 670 nm. The formed state, with an average life-time of 660 ps (red circles), is most likely an intramolecular charge transfer state (ICTS), as the electrons transfer from the excited ICT state, $(P^{\delta-}T^{\delta+})^*$, of **DPP-(2TPhCN)$_2$** to the *p*-cyanophenyl end-group:

$$(P^{\delta-}T^{\delta+})^*C \rightarrow (PT^{\delta+})C^{\delta-},$$

where P = DPP, T = thiophene, and C = the *p*-cyanophenyl unit. The absorption band of the cation radical ($PT^{\delta+}$) has been observed at the wavelength region of 900–1200 nm.[6] The negative amplitude of the component spectrum at 550–700 nm, with the average life-time of 660 ps, corresponds to the recovery of the ground state and the ICTS state, together with the positive amplitude at 900–1100 nm, and they recombine with the same rate.

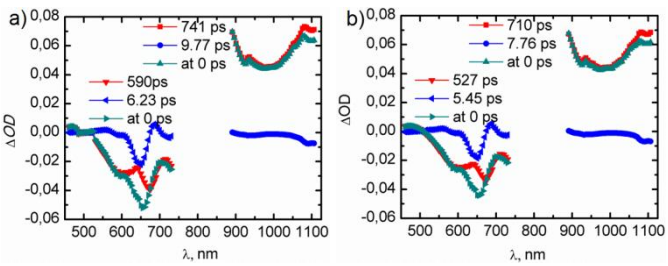

Fig. 14 Transient absorption (green triangles) and decay component spectra (blues and red triangles) of 0.234 mM **DPP-(2TPhCN)$_2$** in the absence (a) and presence (b) of 1.76 mM $PC_{60}BM$ in $CHCl_3$ (λ_{ex} = 650 nm). In pump probe experiments the excitation at 650 slightly alters the shape of the bands at 650 nm.

To estimate the **DPP-(2TPhCN)$_2$**/$PC_{60}BM$ interaction, and the possible electron transfer, the reaction was studied in the presence of 1.76 mM $PC_{60}BM$ in chloroform (Fig. 14b). No remarkable changes, however, appear in the transient spectra. Here, the excitation at 650 nm not only excites the DPP-core, but the $PC_{60}BM$ as well, since it absorbs at that wavelength (See Fig. 12a, curve 7). The only small differences between the spectra in Figures 14a and 14b are the component average lifetimes, 7 ps and 620 ps, which are 5–10% shorter in the presence of $PC_{60}BM$. The differences in lifetimes can be explained rather by the experimental accuracy than by molecular interactions, because $PC_{60}BM$, at the used experimental concentration, 1.76 mM, can not interact with components of lifetimes < 700 ps. This is also one reason, why no evidences for electron transfer from **DPP-(2TPhCN)$_2$** to $PC_{60}BM$ was observed by pump probe experiments. Higher concentrations of $PC_{60}BM$ could not be used, because $PC_{60}BM$ absorbs at 650, and the sample absorbance would exceed the instrumental limit (See Fig. S5).

In the presence of $PC_{60}BM$ the fluorescence of **DPP-(2TPhCN)$_2$** was quenched with the diffusion controlled rate. Because neither traces of the well-known anion radical of $PC_{60}BM$ at about 1100 nm nor new transient species were observed in the pump probe experiments, it seems evident, that there is no electron transfer reaction between the fullerene moiety and **DPP-(2TPhCN)$_2$** in chloroform solution, and that the fluorescence quenching is purely dynamic in nature. Here it is important to note, that according to the time-resolved fluorescence measurements the fluorescence of DPP-core is quenched by only about 5% with the $PC_{60}BM$ concentration used in the pump-probe experiments. In solar cell experiments, the **DPP-(2TPhCN)$_2$**:$PC_{70}BM$ cell produced I_{sc} of -1.20 mA cm^{-2}, and the cells doped with **DPP-(2TPhCN)$_2$** had higher current than the non-doped reference cell. This means that an electron transfer in solid state can not be ruled out.

Interaction between P3HT and **DPP-(2TPhCN)$_2$** was also studied by corresponding steady state and transient absorption measurements. Energy transfer between the molecules was not observed, but electron transfer from P3HT to **DPP-(2TPhCN)$_2$** could be possible (See SI: pages 20-21).

Interaction of di-(p-CNPh)4T with $PC_{60}BM$. As the LUMO level of **di-(*p*-CNPh)4T** (-2.62 eV)[19] is higher than that of $PC_{60}BM$ (-3.7 eV) (Fig. 6), and if **di-(*p*-CNPh)4T** is excited, a photoinduced energy or electron transfer is possible from the former to the latter. In chloroform solution, the emission of **di-(*p*-CNPh)4T** is quenched as a function of $PC_{60}BM$ concentration (Fig. 15 and Table 8). As the emission decay curves (Fig. 15c) show, lifetimes of the single exponential fits decrease in the presence of $PC_{60}BM$. The Stern-Volmer plot (Fig. 15d) shows linear dependency of the fluorescence intensity and lifetime ratios on $PC_{60}BM$ concentration. Since the slopes of the linear fits for the intensity and lifetime ratios are not the same, both dynamic and static quenching are possible in the presence of $PC_{60}BM$.

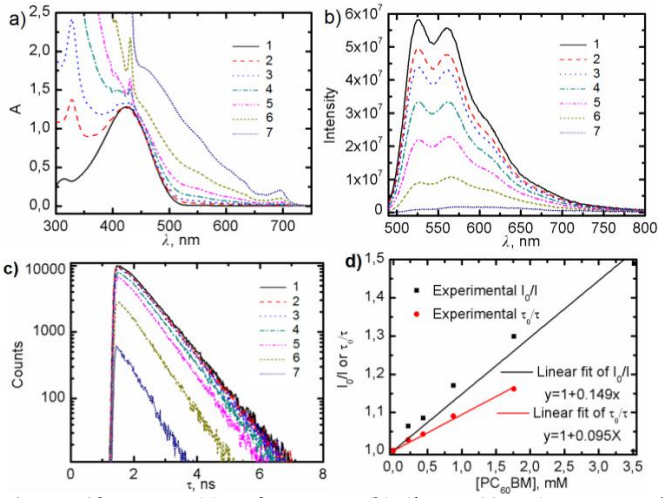

Fig. 15 Absorption (a) and emission (b) (λ_{ex} = 483 nm) spectra and emission decay curves (λ_{ex} = 483 nm and λ_{mon} = 525 nm) (c) and Stern Volmer plot (d) of **di-(*p*-CNPh)4T** with different concentrations of $PC_{60}BM$ (concentrations shown in Table 8).

Next, the kinetics of the photoinduced reactions was studied by the pump-probe method. The excitation took place at the wavelength of 483 nm, which corresponds to the absorption of **di-(*p*-CNPh)4T**. Fig. 16a presents the sum of the decay component spectra of **di-(*p*-CNPh)4T** in chloroform at 0 ps (green curve) and the component spectra with life-times of 1.0–5.1 ps (blue curves) and 700–920 ps (red curves). The first decay component (1.0–5.1 ps, blue triangles) could be an ICT state as electrons spread from the quaterthiophene backbone to the *p*-cyanophenyl groups forming a quaterthiophene cation, analogically to the sexithiophene ($6T^+$) cation, which absorbs[25] around 800 nm, or sexithiophene dication ($6T^{2+}$), which absorbs[26] at 940 nm. The second component (τ = 707–923 ps, red circles) shows the decay of the ICT back to the ground state. The lifetime of the ICT state is consistent with the singlet excited state lifetime of 0.72 ns measured for **di-(*p*-CNPh)4T** by TCSPC.

In the presence of $PC_{60}BM$ the decay component spectra of **di-(*p*-CNPh)4T** does not show changes in the absorption peak positions, but the life-times are slightly decreased (Fig. 16b). They are, however, longer than the corresponding fluorescence lifetimes of **di-(*p*-CNPh)4T**. Here, the longest living transient component in the absence of $PC_{60}BM$ is 0.9 ns, which is too short-lived to be able to react with 1.76 mM $PC_{60}BM$. Larger concentration of $PC_{60}BM$ could not be used, because the sample absorbance increased too high for the method.

Similarly to **DPP-(2TPhCN)$_2$**, energy transfer to $PC_{60}BM$ quenches the singlet excited state of **di-(*p*-CNPh)4T**, but no electron transfer takes place with $PC_{60}BM$ in chloroform solution. As for **DPP-(2TPhCN)$_2$**, no energy transfer from **di-(*p*-CNPh)4T** to P3HT was observed by corresponding steady state and transient absorption measurements of P3HT and **di-(*p*-CNPh)4T**. However, electron transfer from **di-(*p*-CNPh)4T** to P3HT is possible (See SI: pp. 21-22).

Table 8. Concentrations, absorbances at the excitation wavelength, transmittances at the excitation wavelength, measured and corrected fluorescence emission (λ_{ex} = 483 nm) intensities, and fluorescence lifetimes (λ_{mon} = 525 nm) of **di-(*p*-CNPh)4T** (4T) and $PC_{60}BM$ (Q) solutions 1–7 (Fig. 14) in chloroform.

Sol./ curv.	[4T] (mM)	[Q] (mM)	$A_{(483)}$	$T_{(483)}$[a]	$A_{(525)}$[b]	$T_{(525)}$	$I_{(525)}$ (10^7)	I_{corr}[c] (10^7)	τ (ns)
1	0.18	-	0.39	0.64	0.02	0.98	5.8	9.3	0.72
2	0.18	0.22	0.41	0.62	0.05	0.92	5.0	8.7	0.70
3	0.18	0.44	0.46	0.59	0.09	0.87	4.4	8.5	0.69
4	0.18	0.88	0.54	0.54	0.16	0.78	3.3	7.9	0.66
5	0.18	1.76	0.64	0.48	0.28	0.64	2.2	7.1	0.62
6	0.18	3.52	0.93	0.34	0.53	0.42	0.9	6.2	-[d]
7	0.18	7.04	1.57	0.16	1.10	0.17	0.1	3.1	-[d]

[a]Estimated transmittance of the sample solution for the excitation light: $T_{(483)} = 10^{(-1/2\times A(483))}$, as the fluorescence intensity is measured in 90 degree angle relative to excitation, [b]Estimated transmittance of the sample solution for the emitted light at 525 nm: $T_{(525)} = 10^{(-1/2\times A(525))}$, [c]Corrected intensity at 525 nm: $I_{corr} = I_{(525)} / (1-(T_{483}\times T_{525})$, [d]Number of counts too small for a reliable fit

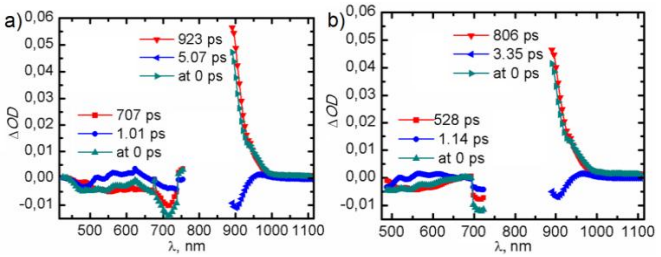

Fig. 16 Transient absorption (green triangles) and decay component spectra (red and blue triangles) of 0.355 mM **di-(*p*-CNPh)4T** in the absence (a) and presence (b) of 1.76 mM $PC_{60}BM$ in chloroform (λ_{ex} = 483 nm).

Experimental section

di-(*p*-CNPh)4T was synthesized as presented in our previous work.[19]

Synthesis of compound 2. DMA (4 mL), toluene (4 mL), distilled water (0.8 mL) and 3-hexylthiophene-2-boronic acid pinacol ester (91.6 mg, 0.311 mmol) were bubbled with argon for 15 min. Compound **1** (100.0 mg, 0.147 mmol), Cs_2CO_3 (216.7 mg, 0.665 mmol) and $Pd(PPh_3)_4$ (20.7 mg, 0.018 mmol) were added to the reaction flask. The reaction mixture was stirred and heated (110 °C) under argon for 2 h. The solvents were evaporated and the crude product was dissolved in toluene. The desired product was isolated as dark blue solid (118 mg, 94%) by column chromatography (SiO_2, toluene). ^{1}H NMR (200 MHz, dichloromethane-d_2) δ ppm 0.82–0.94 (m, 18H), 1.26–1.43 (m, 28H), 1.65–1.72 (m, 4H), 1.90–1.97 (m, 2H), 2.85 (t, *J*=7.50 Hz, 4H), 4.04 (d, *J*=7.55 Hz, 4H), 7.01 (d, *J*=5.29 Hz, 2H), 7.28–7.32 (m, 4H), 8.98 (d, *J*=4.15 Hz, 2H). ^{13}C NMR (101 MHz, dchloromethane-d_2) δ ppm 11.0, 14.4, 14.5, 23.3, 23.8, 24.4, 29.2, 29.9, 30.3, 31.1, 31.2, 32.4, 40.1, 46.7, 109.0, 125.9, 127.2, 129.8, 130.4, 131.3, 136.6, 140.2, 142.1, 142.7, 162.3. HRMS: calcd for $C_{50}H_{69}N_2O_2S_4$ ($[M+H]^+$) 857.4242, found 857.4236.

Synthesis of compound 3. Compound **2** (110.0 mg, 0.128 mmol) was dissolved in chloroform (5.5 mL). NBS (47.8 mg, 0.269 mmol) was added to the reaction flask in one portion. The reaction mixture was irradiated by ultrasound for 1 ½ h at room temperature. The reaction mixture was filtered through a

thin pad of silica gel and rinsed with toluene. The solvents were evaporated and the product was purified by column chromatography (SiO_2, toluene). Compound **3** was collected as dark blue solid (126.5 mg, 97%). ^{1}H NMR (200 MHz, dichloromethane-d_2) δ ppm 0.82–0.92 (m, 18H), 1.26–1.44 (m, 28H), 1.57–1.68 (m, 4H), 1.87–1.93 (m, 2H), 2.79 (t, *J*=7.75 Hz, 4H), 4.01 (d, *J*=8.31 Hz, 4H), 6.98 (s, 2H), 7.24 (d, *J*=4.15 Hz, 2H), 8.96 (d, *J*=4.15 Hz, 2H). ^{13}C NMR (101 MHz, dichloromethane-d_2) δ ppm 11.0, 14.4, 14.4, 23.3, 23.8, 24.4, 29.2, 29.8, 30.3, 31.0, 31.0, 32.3, 40.1, 46.7, 109.2, 112.7, 127.6, 130.3, 132.0, 134.1, 136.5, 140.1, 141.1, 142.7, 162.2. HRMS: calcd for $C_{50}H_{67}N_2O_2S_4Br_2$ ([M+H]$^+$) 1013.2452, found 1013.2430.

Synthesis of compound DPP-(2TPhCN)$_2$. DMA (4 mL), toluene (4 mL) and distilled water (0.8 mL) were bubbled with argon for 15 min. Compound **3** (100.6 mg, 0.099 mmol), 4-cyanophenylboronic acid (30.6 mg, 0.208 mmol), Cs_2CO_3 (146.9 mg, 0.451 mmol), Pd_2dba_3 (5.8 mg, 6.3 μmol) and *t*-$Bu_3P{\cdot}HBF_4$ (7.4 mg, 0.026 mmol) were added to the reaction flask. The reaction mixture was stirred and heated (110 °C) under argon for 3 h. The solvents were evaporated and the product was prepurified by column chromatography (SiO_2, chloroform). The product was boiled in methanol (15 mL) for 30 min. The cooled mixture was filtered and the isolated solid product was washed with methanol (25 mL) and *n*-hexane (15 mL). The procedure gave the desired product as dark purple powder (88.2 mg, 84%). ^{1}H NMR (400 MHz, chloroform-*d*) δ ppm 0.87–0.97 (m, 18H), 1.30–1.46 (m, 28H), 1.75 (quin, *J*=7.59 Hz, 4H), 1.96–1.99 (m, 2H), 2.88 (t, *J*=7.78 Hz, 4H), 4.08 (d, *J*=7.53 Hz, 4H), 7.31 (s, 2H), 7.36 (d, *J*=4.02 Hz, 2H), 7.66–7.71 (m, 8H), 9.01 (d, *J*=4.02 Hz, 2H). ^{13}C NMR (101 MHz, dichloromethane-d_2) δ ppm 11.0, 14.5, 23.3, 23.8, 24.4, 29.2, 30.0, 30.7, 31.0, 31.1, 31.1, 32.4, 40.2, 46.8, 109.3, 111.7, 119.3, 126.4, 127.5, 129.3, 130.3, 132.4, 133.4, 136.7, 138.5, 140.0, 141.4, 141.8, 143.3, 162.1. HRMS: calcd for $C_{64}H_{75}N_4O_2S_4$ ([M+H]$^+$) 1059.4773, found 1059.4772.

Computational methods. Structural and electronic properties of the oligomer were studied using density functional theory (DFT) in conjunction with the hybrid Becke's three-parameter Lee–Yang–Parr exchange-correlation functional (B3LYP)[27,28] and 6-31G** basis set. The optimal dihedral angles of the oligomer were determined with relaxed potential energy surface (PES) scans, in which one dihedral angle (at a time) was changed at 20° intervals between 0° and 180° and the geometry was otherwise fully optimized at each step. The information on the optimal dihedral angles was used to build the final starting geometry of the oligomer, which was then fully optimized in vacuum. The final optimized ground-state oligomer geometry was confirmed to be the minimum-energy structure by a frequency calculation. Time-dependent DFT (TDDFT) calculations were carried out to determine the excited-state vertical transition energies, oscillator strengths, and the UV-Vis absorption spectrum of the oligomer in chloroform for the first 20 excited states using the same DFT functional and the basis set mentioned above. All the calculations were carried out with the Gaussian 09 (Revision C.01) suite of programs[29]. Pictorial presentations of the geometry and frontier molecular orbitals of the oligomer were generated with Chemcraft 1.7[30]. The contributions of molecule fragments to the molecular orbitals were determined with the C-squared Population Analysis (C-SPA)[31].

Spectroscopic measurements. The steady state absorption and fluorescence were measured by employing a UV-3600 Shimadzu UV-VIS-NIR spectrophotometer and a Jobin Yvon-SPEX fluorolog. The fluorescence lifetimes were measured using a time correlated single photon counting (TCSPC) system equipped with a Picoharp 300 controller and a PDL 800-B driver for excitation and a microchannel plate photomultiplier (Hamamatsu R3809U-50) for detection in 90º configuration. The excitation wavelengths were 405 nm and 483 nm and pulse frequency 2.5 MHz. Pump-probe technique for time resolved absorption was used to detect the fast processes with a time resolution shorter than 0.2 ps.

Solar cell preparation. The solvents and Alq_3 (99.995%) were purchased from Sigma-Aldrich and used without further purification. The solar cell samples were prepared on ITO coated glass substrates (1.2 cm × 3.5 cm) purchased from Solems. The zinc-acetate ($Zn(OAc)_2{\cdot}2H_2O$) for ZnO layer preparation was purchased from Sigma-Aldrich. Reference polymer, P3HT, was purchased from Rieke Metals and acceptor $PC_{60}BM$ (99.0%) from Nano-C.

Solar cells were constructed on commercial ITO covered glass substrates. The ITO layer was taped and lacquered for *aqua regia* etching to achieve a patterned ITO. The etched plates were cleaned by sonication in acetone, chloroform, SDS solution (20 mg sodium dodecyl sulphate in 500 mL Milli-Q H_2O), Milli-Q H_2O and 2-propanol (30 min in each), in the previously stated order, and dried under vacuum at 150 ºC for one hour. After a 10 min N_2 plasma cleaning procedure (Harrick Plasma Cleaner PDG-236), a 20 nm ZnO layer was deposited by 1 min spin-coating in WS-400B-6NPP/LITE spin-coater from Laurell Technologies from 50 g L^{-1} zinc-acetate in 96% 2-methoxyethanol and 4% ethanolamine solution following the literature process.[32]

The photoactive layer compounds, P3HT, $PC_{60}BM$/$PC_{70}BM$ and dopant molecules, were dissolved in 1,2-dichlorobenzene (DCB) and stirred (250 rpm) overnight at 50 ºC. Spin-coating of the BHJ photoactive layer from the P3HT:PCBM:dopant blend took 5 minutes (600 rpm) in the spin-coater under N_2 flow. The spin-coated films were annealed under vacuum at 110 ºC for 10 min. Buffer layer and Ag anode were evaporated in the vacuum evaporator under ~ 3×10^{-6} mbar pressure. The evaporation rate and film thickness were controlled with evaporator crystals to deposit the desired thickness of the buffer and ~50 nm thick Ag anode layers on top of the photoactive layer. The cells were stored in the ambient atmosphere in the dark before measurements and analysis.

The photovoltaic parameters were obtained and calculated from current-voltage (*I-V*) curves, which were measured in the dark and under simulated AM 1.5 sunlight illumination (50 mW cm^{-2}) using an Agilent E5272A source/monitoring unit. A voltage of -0.20 V – 0.60 V was applied in 10 mV steps. The measurements were carried out in ambient atmosphere at room temperature without encapsulation of the devices. The cell areas varied between 1 mm^2 and 2 mm^2 were measured by an optical microscope (MBS-10) The illumination was produced by a filtered Xe-lamp (Oriel Corporation & Lasertek) in the Zuzchem LZC-SSL solar simulator. The illumination power density was measured using a Coherent Fieldmax II LM10 power meter. Because a certified measuring system could not be employed, the absolute efficiency values are not directly comparable with the other published results. However, the reported efficiencies and the relative efficiency changes are comparable within the presented devices.

Electrochemical measurements. Differential pulse voltammetry (DPV) measurements were carried out by employing an Iviumstat (Compactstat IEC 61326 Standard) potentiostat and a three-electrode cell configuration to determine HOMO and LUMO energy levels for DPP-(2TPhCN)$_2$. The measurements were carried out using 0.1 M $TBAPF_6$ in dichloromethane (DCM) as supporting electrolyte, glass platinum electrode as working electrode, graphite rod as counter electrode and platinum wire as pseudo reference electrode. For each sample, the background was measured for 2.5 ml of the electrolyte solution after 20 min of deoxygenation purging with N_2. 100 µl of 0.5 mM sample in DCM was inserted and the system was stabilized again by purging with N_2. Each sample was measured between -2.5 V and 2.0 V scanning in both directions with 2.5 mV steps. Ferrocene (Acros Organics, 98%) was used as internal standard reference to scale the measured potentials against vacuum level[33]. HOMO and LUMO level calculations were based on the formal oxidation and reduction potentials observed in the DPV curves according to the following equations:

$$E_{HOMO} = - (4.8 + E_{dif,ox})eV$$
$$E_{LUMO} = - (-E_{dif,red} + 4.8)eV,$$

where 4.8 eV is the oxidation energy of ferrocene. $E_{dif,ox}$ is the difference in volts between the formal oxidation potentials of ferrocene and the measured sample. $E_{dif,red}$ is the difference in volts between the formal oxidation potential of ferrocene and the formal reduction potential of the sample.

Conclusions

DPP-(2TPhCN)$_2$ was synthesized in order to include the DPP-group in the center of the aryl end-capped oligothiophene, **di-(*p*-PhCN)T4**, to broaden its absorption spectrum to the near IR-region. **DPP-(2TPhCN)$_2$** and **di-(*p*-PhCN)T4** molecules were compared as dopant materials in inverted P3HT:$PC_{60}BM$ BHJ organic solar cells. The use of **DPP-(2TPhCN)$_2$** molecules as dopants in the photoactive layer increased the cell efficiency significantly, whereas the increase in the cell efficiency with **di-(*p*-PhCN)T4** doping was minor. Intra- and intermolecular interactions of the two dopant materials with the photoactive layer components, P3HT and $PC_{60}BM$, were studied in chloroform solutions using spectroscopic methods. Fluorescence emission intensity and lifetimes of the **DPP-(2TPhCN)$_2$** and **di-(*p*-CNPh)4T** dopant molecules decreased in the presence of $PC_{60}BM$, but no traces from electron transfer processes were observed in the presence of $PC_{60}BM$. Thus, the emissions of the dopants are quenched by an energy transfer to $PC_{60}BM$ on chloroform solutions.

The cells doped with **DPP-(2TPhCN)$_2$** had higher absorbance than the non-doped reference cell. Inclusion of the dopant molecules broadens the cell absorption to the near IR-region, and the cells with doping absorb at wider wavelength range than the reference cell. Thus, the dopant molecules function as additional light absorbers in the photoactive layer. The doped cells produced current at longer wavelengths, where dopant molecules absorb. Therefore electron transfer from the dopant molecules to $PC_{60}BM$ is possible in solid state, supported also by the produced current of the **DPP-(2TPhCN)$_2$**:$PC_{70}BM$ cell. After excitation, the dopant molecules transfer electrons to $PC_{60}BM$, which increases the cell I_{sc} and power conversion efficiency. Emission of the cells doped with **DPP-(2TPhCN)$_2$** decreased compared to the reference cell due to electron or energy transfer from P3HT to dopant molecules, which further supports decreased amount of recombinations and improved cell performance.

Author contributions

O.E.O.H. and H.J.L. act as group leaders. J.P.H. and D.P. synthesized and characterized all the compounds. V.M.M. performed the spectroscopic, electrochemical, and solar cell studies. T.K. and T.I.H. carried out the computational studies.

Acknowledgements

The authors thank Mrs. Päivi Joensuu for HRMS data. National Doctoral Programme in nanoscience, NGS-NANO, is greatly acknowledged for funding. Funding from the Academy of Finland has enabled the computational work, which is greatly appreciated. Computing resources provided by the CSC – IT Center for Science Ltd, administrated by the Finnish Ministry of Education, are acknowledged.

Notes and references

[a] Department of Chemistry and Bioengineering, Tampere University of Technology, P.O. Box 541, FI-33101, Tampere, Finland. E-mail: *venla.manninen@tut.fi*

[b] Department of Chemistry, P.O. Box 3000, FI-90014 University of Oulu, Finland.

*Electronic Supplementary Information (ESI) available: ^1H and ^{13}C NMR spectra; dihedral angles, DFT optimized ground state geometry and absorption spectrum of **DPP-(2TPhCN)$_2$** calculated at the B3LYP/6-31G** level of theory. See DOI: 10.1039/b000000x/*

[1]a) K. H. Hendriks, G. H. L. Heintges, V. S. Gevaerts, M. M. Wienk and R. A. J. Janssen, *Angev. Chem. Ed.* 2013, **52**, 8341; b) S. Kouijzer, J. J. Michels, M. van den Berg, V. S. Gevaerts, M. Turbiez, M. M. Wienk and R. A. J. Janssen; c) S. Albert-Seifried, D.-H. Ko, S. Hüttner, C. Kanimozhi, S. Pathil and R. H. Friend, *Phys. Chem. Chem. Phys*., 2014, **16**, 6743.

[2]a) G. D. Sharma, M. A. Reddy, K. Ganesh, S. P. Singh and M. Chandrasekham, *RSC Adv*. 2014, **4**, 732; b) M. Chen, W. Fu, M. Shi, X. Hu, J. Pan, J. Ling, H. Li and H. Chen, *J. Mater. Chem. A*, 2013, **1**, 105, c) J. Huang, H. Jia, L. Li, Z, Lu, W. Zhang, W. He, B. Jiang, A. Tang, Z. Tan, C. Zhan, Y. Li and J. Yao, *Phys. Chem. Chem. Phys*. 2012, **14**, 14238; d) B. Walker, A. B. Tamayo, X.-D. dang, P. Zalar, J. Hwa Seo, A. Garcia, M. Tantiwiwat and T.-Q. Nguyen, *Adv. Funct. Mater*. 2009, **19**, 3063.

[3]a) P. Sonar, G.-M. Ng, T. T. Lin, A. Dodabalabur and Z.-K. Chen, *J. Mater. Chem.* 2010, **20**, 3626; b) B. P. Karsten, J. C. Bijleveld and R. A. Janssen, *Macromol. Rapid Commun*. 2010, **31**, 1554.

[4]T. L. Chen, Y. Zhang, P. Smith, A. Tamayo, Y. Li and B. Ma, *ACS Appl. Mater. Interfaces*, 2011, **3**, 2275.

[5]S. Qu, W. Wu, J. Hua, C. Kong, Y. Long and H. Tian, *J. Phys. Chem. C*, 2010, **114**, 1343.

[6]B. P. Karsten, R. K. M. Bouwer, J. C. Hummelen, R. M. Williams and R. A. J. Janssen, *Photochem. Photobiol. Sci.*, 2010, **9**, 1055.

[7]B. P. Karsten, P. P. Smith, A. B. Tamayo and R. A. Janssen, *J. Phys. Chem. A*. 2012, **116**, 1146.

[8]a) T. A. Ford, I. Avilov, D. Beljonne and N. C. Greenman, *Phys. Rev. B: Condens. Matter Mater. Phys*. 2005, **71**, 125212; b) T. Offermans, P. A. van Hal, S. C. J. Meskers, M. M. Koetse and R. A. J. Janssen, *Phys. Rev. B: Condens. Matter Phys*. 2005, **72**, 045213. c) T. A. Ford, H. Ohkita, S. Cook, J. R. Durrant, and N. C. Greenman, *Chem. Phys. Lett.* 2008, **454**, 237.

[9]T. Ameri, P. Khoram, J. Min and C. J. Brabec, *Adv. Mater*. 2013, **25**, 4245.

[10]A. Tolkki, K. Kaunisto, J. P. Heiskanen, W. A. E. Omar, K. Huttunen, S. Lehtimäki, O. E. O. Hormi and H. Lemmetyinen, *Thin Solid Films* 2012, **520**, 4475.

[11]J.-S. Huang, T. Goh, X. Li, M. Y. Sfeir, E. A. Bielinski, S. Tomasulo, M. L. Lee, N. Hazari and A. D. Taylor, *Nature Photonics*, 2013, **7**, 479.

[12]V. M. Manninen, J. P. Heiskanen, K. M. Kaunisto, O. E. O. Hormi and H. J. Lemmetyinen, *RSC Adv*. 2014, **4**, 8846.

[13]S.-Y. Liu, M.-M. Shi, J.-C. Huang, Z.-N. Jin, X.-L. Hu, J.-Y. Pan, H.-Y. Li, A. K.-Y. Jen, H.-Z. Chen, *J. Mater. Chem. A* 2013, **1**, 2795.

[14]Lu, S.; Drees, M.; Yao, Y.; Boudinet, D.; Yan, H.; Pan, H.; Wang, J.; Li, Y.; Usta, H.; Facchetti, A. *Macromolecules* 2013, **46**, 3895.
[15]Jackson, N. E.; Savoie, B. M.; Kohlstedt, K. L.; de la Cruz, M. O.; Schatz, G. C.; Chen, L. X.; Ratner, M. A. *J. Am. Chem. Soc.* 2013, **135**, 10475.
[16]Naik, M. A.; Venkatramaiah, N.; Kanimozhi, C.; Patil, S. *J. Phys. Chem. C* 2012, **116**, 26128.
[17]Thompson, J. D.; Xidos, J. D.; Sonbuchner, T. M.; Cramer, C. J.; Truhlar, D. G. *PhysChemComm*. 2002, **5**, 117.
[18]Bader, R. F. W.; Matta, C. F. *J. Phys. Chem. A* 2004, **108**, 8385.
[19]J. P. Heiskanen, V. M. Manninen, D. Pankov, W. A. E. Omar, T. Kastinen, T. I. Hukka, H. J. Lemmetyinen and O. E. O. Hormi, *Synthesis of aryl end-capped quaterthiophenes applied as anode interfacial layers in inverted organic solar cells*, Submitted Manuscript.
[20]J. Pina, H. D. Burrows, R. S. Becker, F. B. Dias, A. L. Macanita and J. Seixas de Melo, *J. Phys. Chem. B*, 2006, **110**, 6499.
[21]a) ITO work function, see: Y. Zhou, J. Won Shim, C. Fuentes-Hernandez, A. Sharma, K. A. Knauer, A. J. Giordano, S. R. Marder and B. Kippelen, *Phys. Chem. Chem. Phys.*2012, **14**, 12014; b) ZnO, P3HT and $PC_{60}BM$ HOMO and LUMO levels, see: A. K. K. Kyaw, X. W. Sun, C. Y. Jiang, G. Q. Lo, D. L. Zhao and D. L. Kwong, *Appl. Phys. Lett.* 2008, **93**, 221107; c) HOMO and LUMO levels of Alq_3, see: A. Tolkki, K. Kaunisto, J. P. Heiskanen, W. A. E. Omar, K. Huttunen, S. Lehtimäki, O. E. O. Hormi and H. Lemmetyinen, *Thin Solid Films*, 2012, **520**, 4475; d) Work function of AgO, see: M. S. White, D. C. olson, S. E. Shaneen, N. Kopidakis and D. S. Ginley, *Appl. Phys. Lett*. 2006, **89**, 143517.
[22]M. C. Schaper, D. Mühlbacher, M. Koppe, P. Denk, C. Waldauf, A. J. Heeger, C. J. Brabec, *Adv. Mater*. 2006, **18**, 789.
[23]J. R. Lakowicz, *Principles of fluorescence spectroscopy 3rd ed*. 2006, University of Maryland School of Medicine, 953 pages.
[24]M. Eschle, Photochemical and Photophysical properties of diketopyrrolopyrrole organic pigments, Lausanne: EPFL, Theses N° 1616, 1997, 130 pages.
[25]a) V. Wintgens, P. Valat and F. Garnier, J. Phys. Chem. 1994, **98**, 228 .
[26]R. A. J. Janssen, L. Smilowitz. N. S. Sariciftci and D. Moses, *J. Chem. Phys*, 1995, **101** (3), 1787.
[27]Becke, A. D. *J. Chem. Phys*. 1993, **98**, 5648.
[28]Lee, C.; Yang, W.; Parr, R. G. *Phys. Rev. B.* 1988, **37**, 785.
[29]*Gaussian 09*, Frisch, M. J. Trucks, G. W. Schlegel, H. B. Scuseria, G. E. Robb, M. A. Cheeseman, J. R. Scalmani, G. Barone, V. Mennucci, B. Petersson, G. A. Nakatsuji, H. Caricato, M. Li, X. Hratchian, H. P. Izmaylov, A. F. Bloino, J. Zheng, G. Sonnenberg, J. L. Hada, M. Ehara, M. Toyota, K. Fukuda, R. Hasegawa, J. Ishida, M. Nakajima, T. Honda, Y. Kitao, O. Nakai, H. Vreven, T. Montgomery, J. A. J. Peralta, J. E. Ogliaro, F. Bearpark, M. Heyd, J. J. Brothers, E. Kudin, K. N. Staroverov, V. N. Kobayashi, R. Normand, J. Raghavachari, K. Rendell, A. Burant, J. C. Iyengar, S. S. Tomasi, J. Cossi, M. Rega, N. Millam, J. M. Klene, M. Knox, J. E. Cross, J. B. Bakken, V. Adamo, C. Jaramillo, J. Gomperts, R. Stratmann, R. E. Yazyev, O. Austin, A. J. Cammi, R. Pomelli, C. Ochterski, J. W. Martin, R. L. Morokuma, K. Zakrzewski, V. G. Voth, G. A. Salvador, P. Dannenberg, J. J. Dapprich, S. Daniels, A. D. Farkas, Ö. Foresman, J. B. Ortiz, J. V. Cioslowski, J. Fox, D. J., Revision C.01, Gaussian, Inc.,Wallingford CT, 2010.
[30]Zhurko, G. A. Chemcraft version 1.70. http://www.chemcraftprog.com.
[31]P. Ros and G. C. A. Schuit *Theo. Chim Acta*. 1966, **4**, 1.
[32]M. S. White, D. C. Olson, S. E. Shaheen, N. Kopidakis and D. S. Ginley, *Appl. Phys. Lett*., 2006, **89**, 143517.
[33]R. R. Gagne, C. A. Koval, G. C. Lisensky, *Inorg. Chem*. 1980, **19**, 2854.

Graphical abstract

Synthesis and properties of **DPP-(2TPhCN)$_2$** dopant molecules, which absorb light and transfer energy to $PC_{60}BM$ increasing the BHJ cell efficiency.